RADIATION EFFECTS IN THE ACOUSTIC

LOSS SPECTRA OF AT-CUT TOYO

QUARTZ CRYSTAL

By

HO BYONG HWANG

Bachelor of Science

Jeonbug National University

Jeonju, Jeonbug, Korea

1974

Submitted to the Faculty of the Graduate College
of the Oklahoma State University
in partial fulfillment of the requirements
for the Degree of
MASTER OF SCIENCE
May, 1985

RADIATION EFFECTS IN THE ACOUSTIC

LOSS SPECTRA OF AT-CUT TOYO

QUARTZ CRYSTAL

Thesis Approved:

*Joel J. Martin*
Thesis Adviser

*George S. Dixon*

*Larry E. Halliburton*

*Norman N. Durham*
Dean of the Graduate College

## ACKNOWLEDGEMENTS

I would like to take this opportunity to thank the members of my committee, Profs. Joel J. Martin, Larry E. Halliburton, and George Dixon for their generous help and advice.  Special thanks are due to Dr. Joel J. Martin, my major adviser and committee chairman, for his advice, suggestion, help, and patience, without which this thesis would not have been completed.  My appreciation also goes to Dr. Harish Bahadur for his help and assistance.

Further acknowledgement is extended to the Solid State Science Division, the Rome Air Development Command, U.S. Air Force Hanscom AFB which sponsored this work.

Lastly I must thank my parents for their understanding and encouragement and my wife, Meeyoung, for the typing of this thesis and her sacrifice.

TABLE OF CONTENTS

LIST OF FIGURES

CHAPTER I

INTRODUCTION

Quartz

$SiO_2$ has several crystalline phases as well as an amorphous phase.
$\alpha$-quartz, sometimes called "low-quartz," is the common phase at temperatures below $573^{\circ}C$. We are concerned with $\alpha$-quartz and will refer to it simply as "quartz." If it is between $573^{\circ}C$ and $870^{\circ}C$, it is called $\beta$-quartz or "high-quartz" which has a hexagonal structure instead of trigonal structure of $\alpha$-quartz. Among the other forms of $SiO_2$ are tridymite, cristobalite, and silica (the fused amorphous form). Both right-handed and left-handed $\alpha$-quartz are found in nature. They are mirror images each other. The Brothers Pierre and Jacques Curie discovered piezoelectricity in 1880. Piezoelectricity can be defined as the electric field generated by mechanical stress especially in a crystalline substances, as quartz, which is referred to as the direct piezoelectric effect. The inverse piezoelectric effect is the stain caused by an applied electric field. By using the piezoelectric properties of quartz, in 1916 Paul Langevin made quartz transducers for ultrasonic submarine detection. About the same time the piezoelectric resonator was developed, and quartz proved to be the most suitable material [1]. This resonator vibrates over an extremely narrow range of frequencies. Quartz crystal can be used as an oscillator or a filter which operates with a combination of the direct and inverse piezoelectric

1

effects.

For a frequency control devices, the quartz stone is cut into plates which become the frequency-determining elements. The simplest slab is an X-cut or Y-cut plate which is perpendicular to an X-axis or Y-axis respectively. These plates can have a number of modes of vibration and, often, each mode will have a different temperature dependence. The X- and Y-cuts have relatively poor temperature-frequency characteristics. Rotated cuts were developed to improve the poor temperature-frequency characteristics of the X- and Y-cuts. The most common modern-day crystal is a rotated Y-plate called the AT-cut. The AT-cut is a Y-cut plate containing the X-axis and rotated about the X-axis by approximately $35^{\circ}20'$. The primary vibration is a thickness-shear mode with atomic displacements in the X-direction. Since the AT-cut crystals are normally excited by electrodes placed on opposite sides of the plate, they operate only on their odd overtones. The frequency of such a resonator is given by [2]

$$f_n = \frac{n}{2t} \left( \frac{C_{66}'}{\rho} \right)^{\frac{1}{2}}$$

where t is the crystal thickness, $\rho$ the density, n the overtone, and $C_{66}'$ the effective elastic constant, which can be written in terms of the actual elastic constants for rotated Y-cut as follows

$$C_{66}' = C_{66} \cos^2\theta + C_{44} \sin^2\theta - C_{14} \sin 2\theta$$

The rotation angle of $35^{\circ} 20'$ about the X-axis is chosen so that the temperature coefficient of the frequency

$$\alpha_T = \frac{1}{f} \frac{\partial f}{\partial T}$$

is zero or very small at the desired operating temperature which is usually between 25$^{\circ}$C and 70$^{\circ}$C.

Point defects produce anelasticity through a stress-induced ordering, which is an example of a relaxation process, i.e., a process involving a time-dependent approach to a new equlibrium strain state as a result of a change in the applied stress. In the case of the sinusoidally oscillating type of experiment, the strain will lag behind the applied stress by a phase angle $\phi$ in an anelastic system. This phase angle $\phi$ is found to be

$$\tan \phi = \frac{1}{2\pi} \frac{\Delta W}{W} \tag{1}$$

where $\Delta W$ is the energy density dissipated in a full cycle and W is the maximum stored energy density [3]. Equation (1) shows that $\tan \phi$ is a measure of the energy dissipated or energy loss in a cycle due to the anelasticity of the material. The quantity $\phi$ (or $\tan \phi$ ) is often called the "internal friction" or the "acoustic loss." The quality factor, Q, of a vibrating system is defined as

$$Q = 2\pi \frac{W}{\Delta W} \tag{2}$$

so long as the damping is small [4], and Equation (1) can be rewritten as follows

$$\phi = Q^{-1} = \frac{1}{2\pi} \frac{\Delta W}{W} \quad , \quad \phi \ll 1 \tag{3}$$

This electro-mechanical oscillatory system can be described by an analog electrical network consisting of a series R, L, C, circuit shunted by a second capacitance $C_1$ as shown in Figure 1. The motional R, L, C
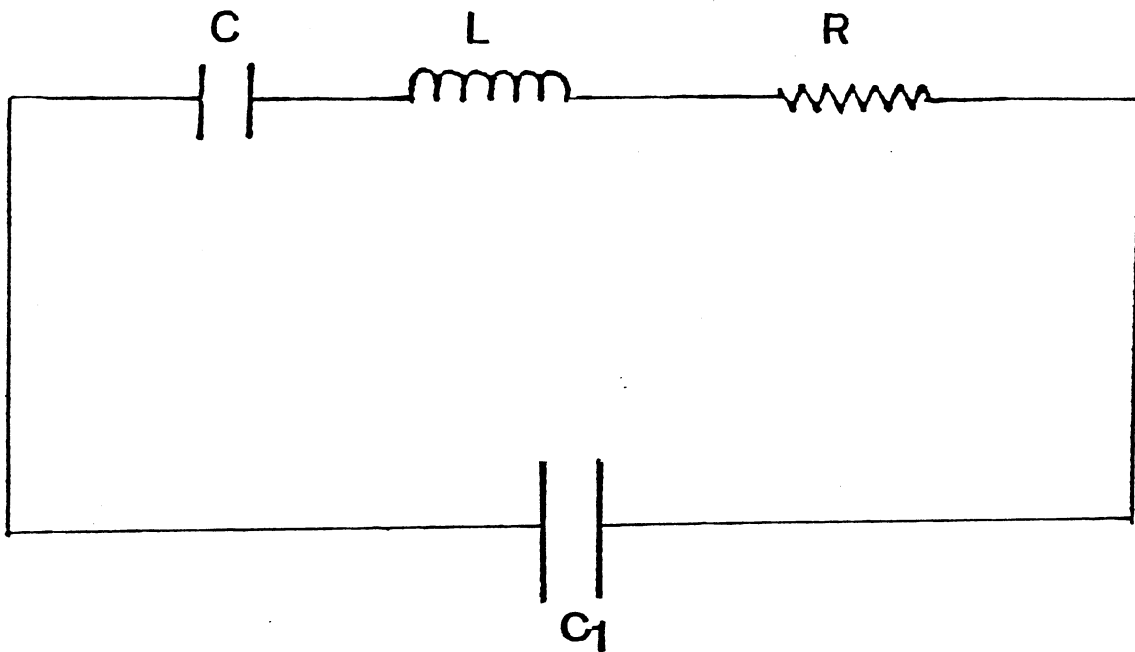
Figure 1. Electrical Equivalent of a Quartz Crystal Resonator

elements describe the mechanical vibrational part while $C_1$ is caused by the electrodes and associated cables. The Q factor of the oscillating system can be expressed in terms of the equivalent electrical constants as the following [1]

$$Q = \frac{\omega L}{R} \tag{4}$$

where $\omega$ is an oscillating frequency in the neighborhood of a natural frequency.

The measurement of acoustic loss as a function of temperature is a useful technique for the identification of point defects in both natural and synthetic quartz crystals. This measurement also provides a direct connection to the performance of the crystal in an oscillating circuit. The losses are caused by an interaction of the crystal vibration with the thermal phonons. The phonon-phonon interactions are related to the anharmonic character of the solid. The loss due to the phonon-phonon interactions is the expression of the anharmonic character of the solid, and determines the background loss in a perfect crystal containing no impurities. A general acoustic loss vs temperature spectrum is shown in Figure 2. The dashed line is the background due to phonon-phonon inter-actions and as is the 20K loss peak. The solid line is the result of the superposition of the background loss and the effects of impurities. Both the strong 54K loss and the weak 135K loss are caused by the $Al-Na^+$ center. The exponentially increasing loss above 450K is due to the diffusion of alkali ions in the crystal and the magnitude of this loss contribution is dependent on the type of alkali present and their con-centration.

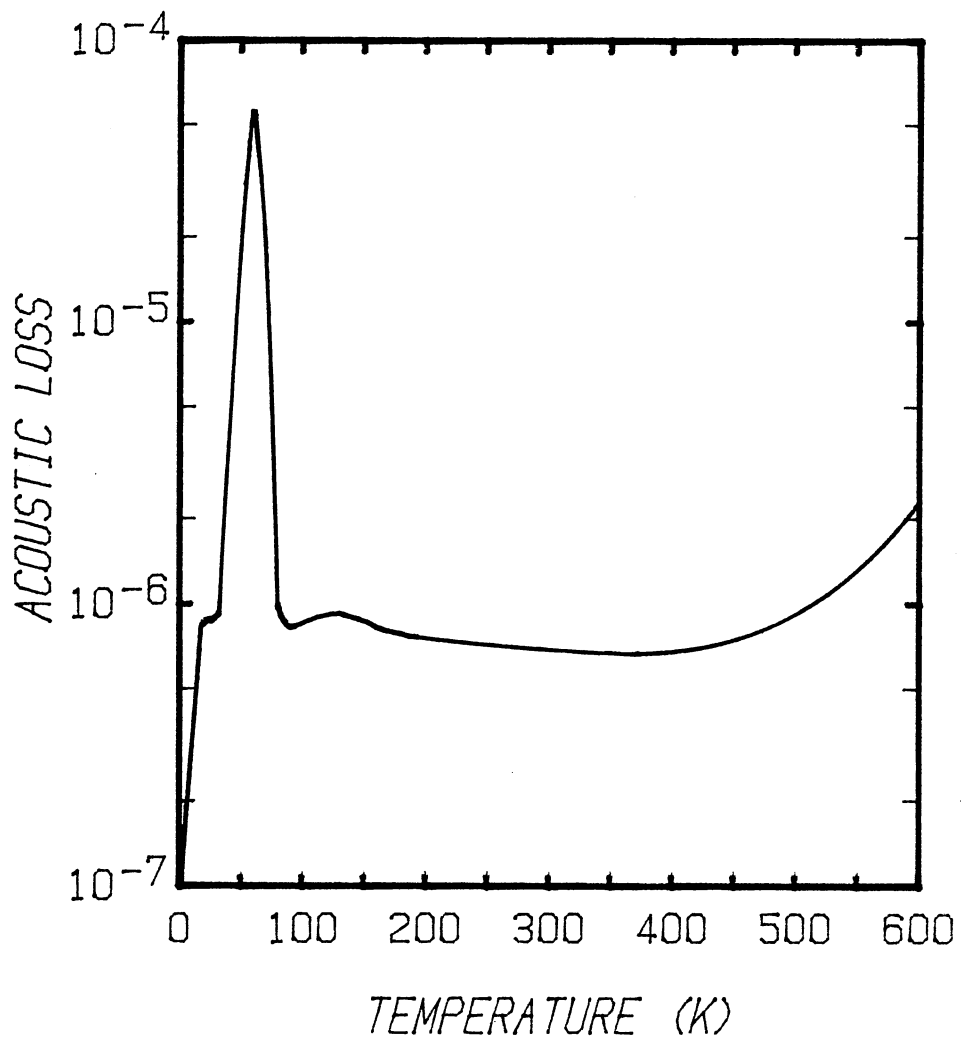H. E. Bömmel, W. P. Mason, and A. W. Warner [5, 6] first found the

Figure 2. A General Figure of the Acoustic Loss

two loss peaks, one near 20K and the other near 50K in 5MHz AT-cut quartz resonators. J. C. King [7,8] introduced annealing, electrolysis and irradiation techniques. He found another loss peak near 135K in quartz containing a large 50K loss peak. He also found that electrolysis removed the 50K loss peak and induced a 85K loss peak. C. K. Jones and C. S. Brown [9] reported that the 50K loss was increased and the 20K peak decreased with increasing growth rate of the quartz stone. D. B. Fraser [10] diffused the various alkali ions into resonators by electrodiffusion technique. He found the 50K and 135K loss peaks with the $Na^+$-diffused natural quartz which was similar to those of the synthetic z-minor quartz. The $Li^+$-diffused resonator showed a reduction of the 50K loss peak while the $K^+$-diffused resonator showed the large 50K loss peak. This last result is understandable because the $Na^+$ ions present at the furnace or the anode material could move more readily in the case of electrodiffusion of the large $K^+$ ions than in the case of the $Li^+$-diffusions. J. C. King [7,8] and Fraser [10] showed that the $Al-Na^+$ center is responsible for the 54K loss peak by using irradiation and electrodiffusion techniques. J. J. Martin [11] swept $Li^+$ and $H^+$, or $D^+$ into AT-cut resonators made from high-aluminum-content Premium Q grade quartz and measured the acoustic loss in the temperature range from 4.5K to 370K. The small 54K loss peak present in the as-received sample was removed by the electrodiffusion but no new loss peaks were introduced in this temperature range. Therefore, he concluded that the $Al-Li^+$ and the $Al-OH^-$ centers have no acoustic loss peaks in this temperature region.

J. C. King [7,8] found that the size of the 50K loss peak was reduced and a new 100K loss peak was produced after irradiating the

resonators with 50KV x-rays.  King and Sander [12] produced the 100K

loss and the broad loss peak between 125K and 165K by irradiating the

AT-cut resonator at liquid nitrogen temperature and measuring the losses

as the resonator was warmed up, and attributed these loss peaks to the

Al-hole center.  J. J. Martin, L. E. Halliburton, and R. B. Bossoli [13]

described this broad loss as a single peak centered at 135K.  J.J. Martin

and S. P. Doherty [14] suggested that the 23K peak is also due to the

Al-hole center.  Infrared studies by W. A. Sibley, J. J. Martin, and

M. C. Wintersgill et al. [15] and ESR studies by M. E. Markes and L. E.

Halliburton [16] on well-characterized synthetic quartz show that in the

presence of an ionizing radiation field, hydrogen is mobile at all tempe-

ratures; but sodium and the other alkalis are mobile only at the tempera-

tures above 200K.  Acoustic loss studies under irradiation by Doherty and

Martin [17] also show that sodium become mobile above 200K.  L. E. Halli-

burton, N. Koumvakalis, and M. E. Markes et al. [11] reported that the

room temperature irradiation breaks up the Al-Na$^+$ centers and produced a

mixture of the Al-hole and Al-OH$^-$ centers.  They suggested that these

radiation-induced Al-hole centers are responsible for acoustic loss peaks

at 23K, 100K, 135K.


## Internal  Friction


When a stress is applied to a solid, the orientation of point

defects changes with time to a new equilibrium state. This process, known

as "stress-induced ordering," produces the anelastic behavior of the

solid [18].  Acoustic loss or internal friction is a measure of an-

elasticity.  An ideal elastic solid satisfies the following conditions;

an unique equilibrium relation, "instantaneous," and "linearity."

However, if among these three conditions, the condition, "instantaneous,"

is discarded and time-dependence is introduced, the solid is anelastic.

Nowick and Berry have reviewed the theory of anelasticity [3]. In the case of the dynamic experiments such as where the stress and the strain change sinusoidally, the complex elastic modulus $M^*$ of an anelastic solid can be written as

$$M^* = |M| \cdot e^{i\phi} = M_1 + i M_2 \tag{5}$$

where $\phi$ is the loss angle, $M_1$ describes the "storage," and $M_2$ the "loss." The internal friction then follows, from the above Equation (5).

$$\tan \phi = M_2 / M_1 \tag{6}$$

Suppose that the solid "relaxes" at a rate $\tau$ from its unrelaxed state with modulus $M_u$ to a relaxed state with modulus $M_r$ upon the application of a step function stress. Nowick and Berry [3] showed that in the case of small loss angle

$$M_1 = M_u - \frac{\delta M}{1 + \omega^2 \tau^2} \quad , \quad M_2 = \frac{\delta M \, \omega \tau}{1 + \omega^2 \tau^2} \tag{7}$$

where $\delta M = M_u - M_r$ . Figure 3 shows the real $M_1$ and imaginary $M_2$ parts of the complex elastic modulus $M^*$ plotted against the logarithm of $\omega\tau$ . They also showed that the acoustic loss or internal friction for the case of small losses can be written as follows

$$Q^{-1} = \phi = \frac{\Delta \omega \tau}{1 + \omega^2 \tau^2} \tag{8}$$

where $\Delta$ , which is called "relaxation strength," is defined as $\Delta = \delta M / M_u$ . For the case of point defects, the anelastic behavior of a solid often shows a single relaxation process, and follow a single
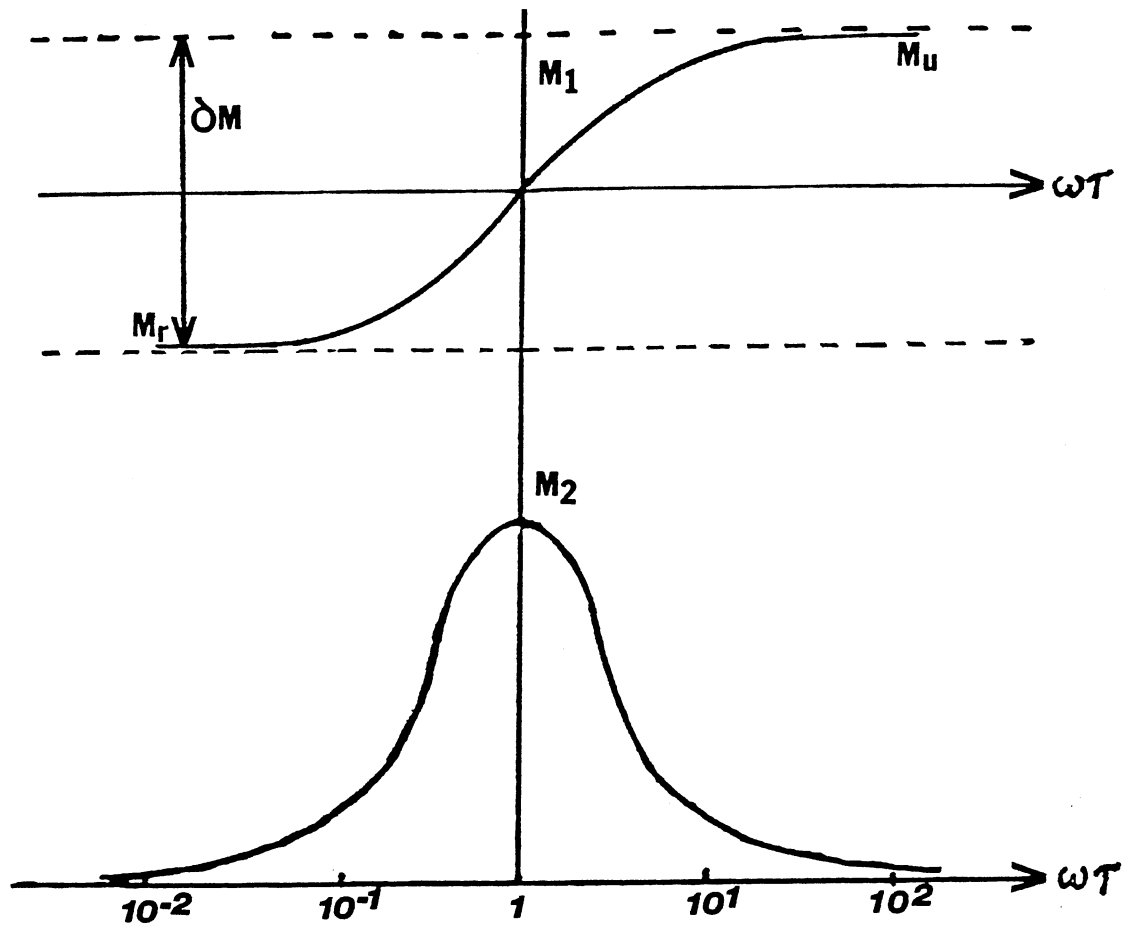
Figure 3. The Variation of $M_1$ and $M_2$ as a Function of Angular
Frequency $\omega$ , where $M_1$ and $M_2$ are the Real and Imaginary
Parts of the Complex Elastic Modulus $M^*$ of an Anelastic
Solid

Debye peak such as Equation (8). Often the relaxation process is due to the thermally activated jumping of an atom or defect between equivalent orientations. When this assumption holds, the probability of a jump per second, $\tau^{-1}$, can be described by an Arrhenius relation;

$$\tau^{-1} = \tau_0^{-1} \exp \left( -\Delta H / k T \right) \tag{9}$$

where $\tau_0^{-1}$ is the product of a vibrational frequency and an entropy factor, $\Delta H$ the height of the potential barrier between the equivalent sites, $k$ Boltzmann's constant, and T the absolute temperature. Acoustic loss measurements are usually made with the sample vibrating on one of its normal modes. Thus, instead of varying $\omega$ , $\tau$ can be varied over a wide range by changing the temperature. Figure 4 shows $M_1$ and $M_2$ plotted as a function of temperature with fixed $\omega$ . One way to obtain the activation energy is to measure the loss versus temperature spectrum for a number of harmonically related modes at $T_p$. Equation (9) can be rewritten as follows

$$\ln \omega = \ln \tau_0^{-1} - \frac{\Delta H}{k} \frac{1}{T_p} \tag{10}$$

So a plot of $\omega$ versus $1 / T_p$ should yield a straight line of slope, $-\Delta H / k$. Another method is to numerically fit Equation (8) with Equation (9) to the experimental loss versus temperature curve at one frequency.

A common way to measure the acoustic loss or internal friction of a sample is to drive it on one of its normal modes of vibration, remove the drive and then measure the free decay of the amplitude. The vibration of this free decay can be expressed by the equation of motion
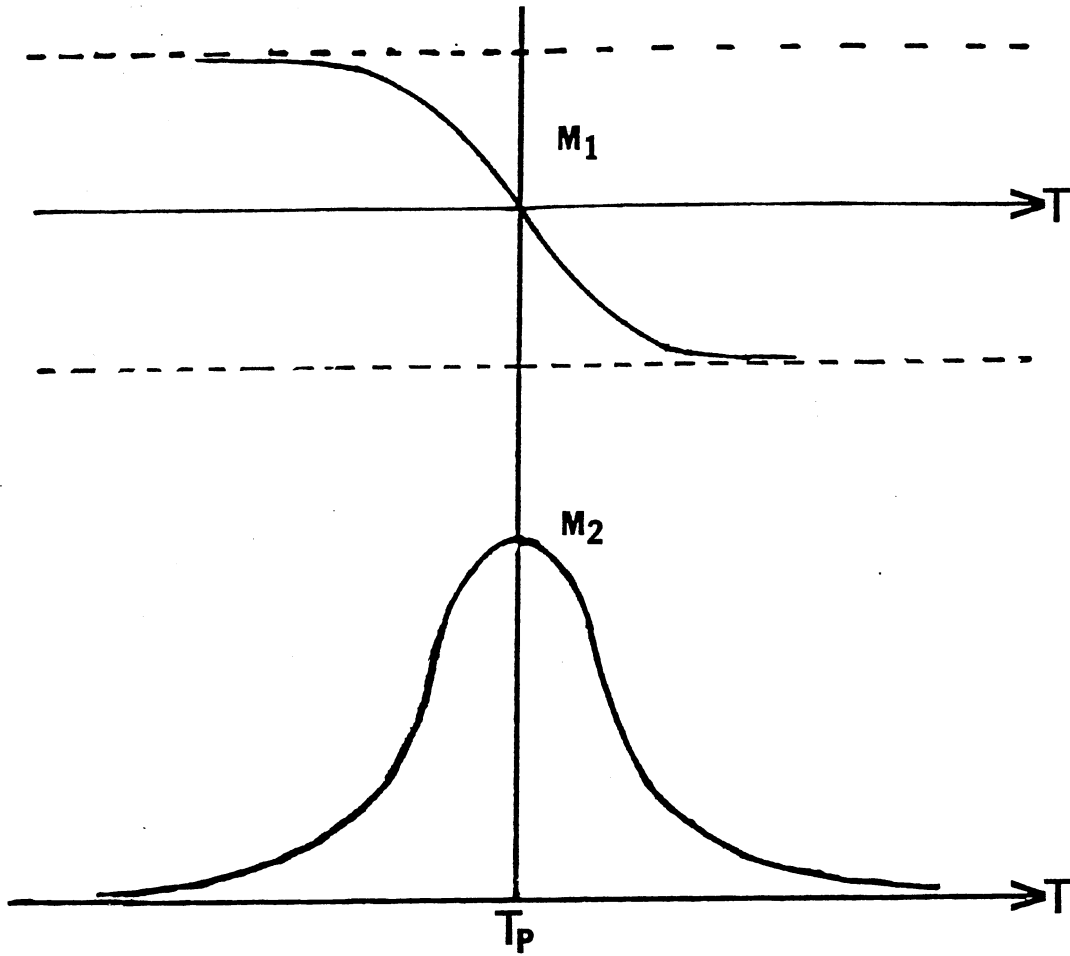
Figure 4. The Variation of $M_1$ and $M_2$ as a Function of Temperature

describing an one-dimensional anelastic spring such as, according to Nowick and Berry [3],

$$m \ddot{x} = - k^* x = - k_1 \cdot ( 1 + i \tan\phi ) x \qquad (11)$$

where m is the mass attached to the end of the anelastic spring, $k^*$ a complex spring constant, $\phi$ the loss angle, $k_1$ is a constant. The solution to Equation (11) is found to be

$$x = x_0 \exp \left[ - \sqrt{\frac{k_1}{m}} \left( \frac{\tan\phi}{2} - \frac{3\tan^3\phi}{48} + \cdots \right) t \right] \cdot$$

$$\exp \left[ i \sqrt{\frac{k_1}{m}} \left( 1 + \frac{\tan^2\phi}{8} + \cdots \right) t \right] \qquad (12)$$

When the loss angle $\phi$ is very small, the natural angular frequency $\omega_0$ in free decay becomes simple; that is $\omega_0 = \sqrt{\frac{k_1}{m}}$. Equation (12) can be rewritten as follows

$$x = x_0 \exp \left[ - \omega_0 \frac{\phi}{2} t \right] \exp \left[ i \omega_0 t \right] , \qquad \phi \ll 1 \qquad (13)$$

If a piezoelectric sample resonator is driven at its resonant frequency and then allowed to freely decay, the decaying voltage will decrease exponentially as

$$V = V_0 \exp ( - t / t_0 ) \exp ( i \omega_0 t ) \qquad (14)$$

where $t_0$ is the relaxation time. Comparing the damping term in Equation (14) with that of Equation (13), we find that

$$\phi = \frac{1}{\pi f_0 t_0} \qquad (15)$$

where $f_0 = \frac{\omega_0}{2\pi}$ is used. When we measure the time $t_{\frac{1}{2}}$ taken for the amplitude of vibration to fall to a half of its initial value, the

relaxation time $t_o$ is found to be

$$t_o = \frac{T_{\frac{1}{2}}}{0.693} \tag{16}$$

Combining Equation (3), Equation (15) and Equation (16), we can write the acoustic loss as follows

$$Q^{-1} = \phi = \frac{0.693}{\pi f_o T_{\frac{1}{2}}} \quad , \qquad \phi \ll 1 \tag{17}$$

where $f_o$ is a tuned frequency and $T_{\frac{1}{2}}$ is obtained from the timer.

## The Purpose of the Investigation

Quartz crystals are often used in electronic insturments as filters and frequency control devices. The performance of such electronic devices in space can be degraded by ionizing radiation [12]. Irradiation at room temperature destroys the $Al-M^+$ centers in quartz and produces a mixture of the Al-hole and $Al-OH^-$ centers [21]. The frequency shift caused by the removal of the $Al-Na^+$ centers and by the production of the Al-hole center is not desirable. Thus, it is very important to know how the defects are modified or produced by the ionizing radiation. Radiation-induced loss peaks at 23K, 100K, and 135K appear to be related to the Al-hole centers while the $Al-Li^+$ and $Al-OH^-$ centers do not show acoustic loss peaks below 370K [11]. A pulsed-electron irradiation technique was primarily used to investigate the destruction of the $Al-Na^+$ centers versus the production of the Al-hole centers as a function of radiation dose. The dependence of the Al-hole center to the $Al-Na^+$ center upon radiation dose was determined by monitoring the 54K loss peak for the $Al-Na^+$ center and the 23K loss peak for the Al-hole center. Measurements were also made using a $^{60}C_o$ gamma source. These data are useful for predicting the radiation response of a quartz oscillator.

# CHAPTER II

## EXPERIMENTAL PROCEDURE

### Method of Measurements

The acoustic loss of the 5MHz third overtone resonator blanks was
determined by using the log-decrement technique.  The blank was held in
a gap holder so as to minimize losses due to the mounting sturucture.
Figure 5 shows the aluminum gap holder which has a printed circuit board
electrode.  The electrodes are seperated by about 0.010 inches from the
surface of the blank.  The gap holder with the sample crystal is threaded
onto the cold finger of a variable temperature liquid helium cryostat.

The variable temperature helium dewar is shown schematically in
Figure 6.  It consists of a cold finger and heater, a heat leak chamber,
an inner helium chamber, an outer nitrogen chamber, and a thin-walled
stainless steel enclosure which is connected to a vacuum system.  The
inner dewar, outer dewar, and stainless steel enclosure are insulated
from each other and the surroundings by the vacuum of at least $5 \times 10^{-6}$
Torr.  The sample can be thermally connected or disconnected to the
cryogenic fluid in the inner dewar by filling the heat leak chamber with
a small amount of helium gas at room temperature or by removing the
helium gas, heat exchange medium, from it.  The heater system consists
of a $14\,\Omega$ constantan wire wound on the cold finger and a HP 6201B DC
power supply.  A model DRC-80C digital cryogenic thermometer/controller
with a model DC-500-DRC silicon diode sensor from Lake Shore Cryotronics,
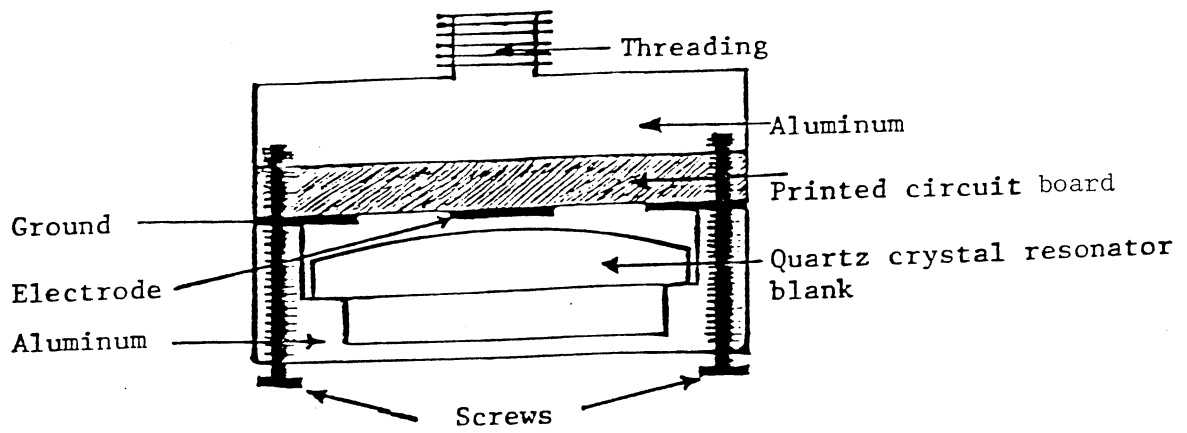
Figure 5. Arragement showing Mounting of a Quartz Crystal Resonator
Blank in a Gap Holder

To mechanical pump

Liquid N$_2$

To pump

Outer Dewar

Thin-walled
stainless steel
enclosure

Inner Dewar

Liquid Helium

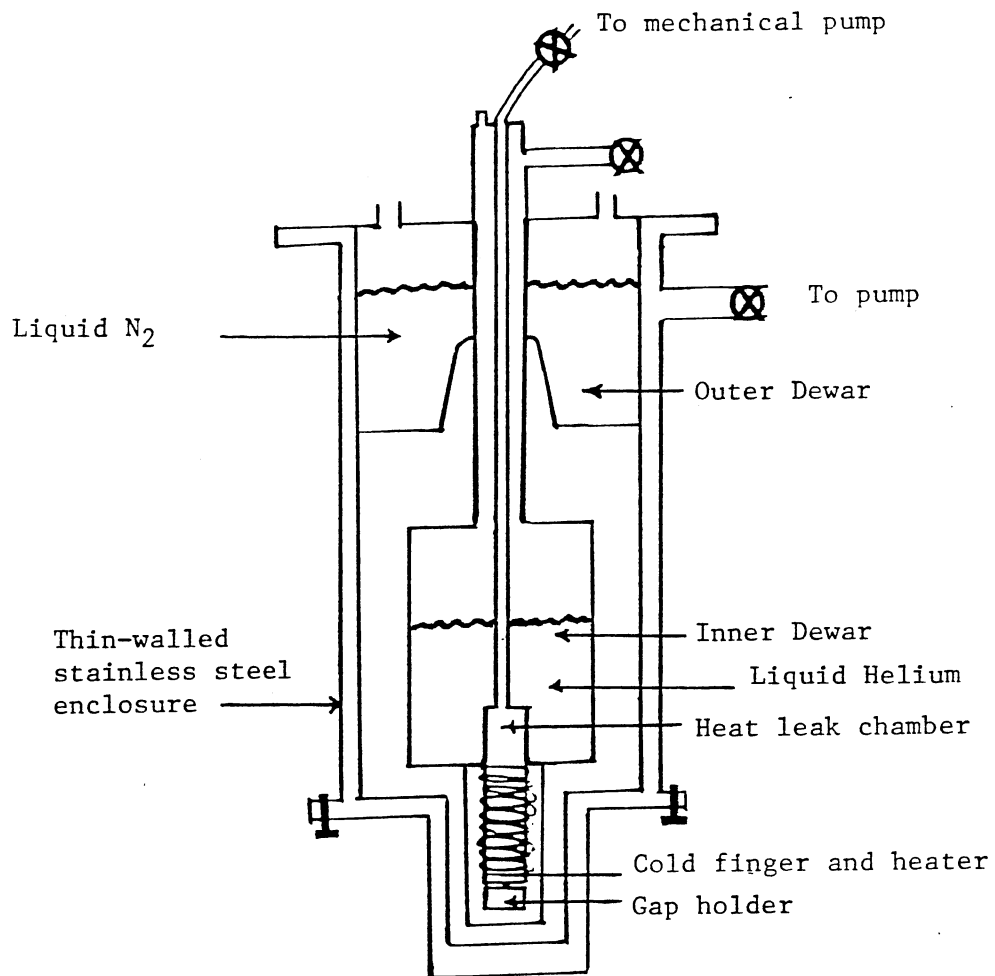Heat leak chamber

Cold finger and heater

Gap holder

Figure 6.  A Variable Temperature Helium Dewar

Inc. were used to monitor the sample's temperature.

To cool down the sample from room temperature to 4.5K, liquid nitrogen was poured into the inner and outer dewars after the heat leak chamber was filled with a helium gas. When the whole system reached equilibrium at 80K, the liquid nitrogen was removed from the inner dewar and then liquid helium was transferred. The holder and resonator blank then cooled to approximately 4.5K. Data were taken starting at low temperatures and then going up in high temperatures. The temperature was raised by applying heater current and reducing the helium pressure in the heat leak chamber. Once 20K was reached the heat leak chamber was pumped continuously and current was increased to bring the sample to the desired temperature.

A schematic diagram of the acoustic loss measuring system is shown in Figure 7. The radio frequency ($f_o \approx$ 5MHz) signal from a HP 3325A synthesizer/function generator goes to the gate which is opened for 10 ms every 0.5, 1, 2, or 5s by the gate control. The sample resonator is driven at its resonant frequency and then allowed to freely decay. This decaying rf ($f_o \approx$ 5MHz) signal is fed into the mixer after amplification by a wide-band pre-amplifier, and there mixed with the rf ($f_o \pm$ 455KHz) signal from the local oscillator. The mixer output, which is 455KHz, is amplified by the two stage intermediate frequency amplifier. This decaying lF signal is rectified with a precision operational amplifier detector and displayed on a Tektronix 5441 storage oscilloscope. The rectified signal from the detector also goes to a pair of level detectors which start the timer function of a HP 5326A timer-counter at 8V and stop it at 4V. Hence the timer reading yields the half-time $t_{\frac{1}{2}}$ of the exponential decay. The acoustic loss, $Q^{-1}$, is
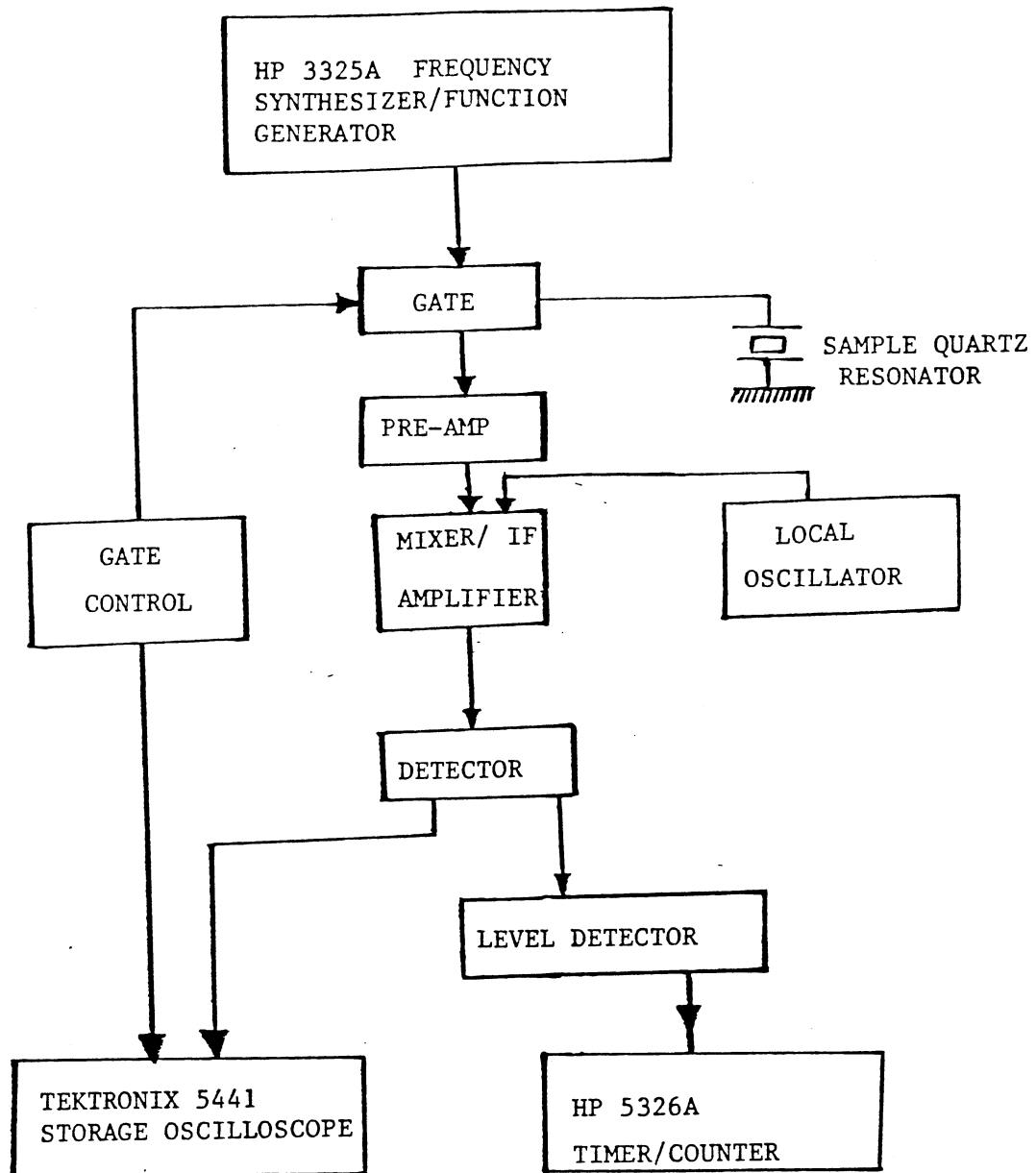
Figure 7. A Schematic Diagram of the Acoustic Loss Measuring System

calculated from Equation (17).

## Description of Sample

Toyo supreme Q labeled bar, SQ-B, of Z-growth synthetic quartz contains approximately 10 to 15 ppm aluminum as impurities.
The substitutional aluminum is compensated by the interstitial alkali, $Na^+$ or $Li^+$, for electrical neutrality [21]. From the OSU supplied Toyo bar, SQ-B, the 14 mm diameter 5MHz third overtone resonator blank was manufactured by Frequency Electronics,Inc. It is a plano-convex shaped AT-cut so that the loss measured is characteristic of the quartz rather than of its mounting structure.

## Radiation Technique

A Van de Graaff electrostatic accelerator was used to irradiate the sample. The holder with the sample was removed from its mounting and carefully wrapped with a piece of household aluminum foil of thickness 0.033mm. The sample was placed 5" in front of the aluminum window of the accelerator.

Irradiations were carried out at room temperature with a 1.75 MeV electron beam. The current density was 10 $\mu$A/cm$^2$ on the sample. The irradiation time was controlled by a Gralab Model 900 programable timer, which made the pulsed-electron possible.

In the first and second irradiations, the Gralab timer was not used and the sample was irradiated for consecutive two and four seconds respectively. From the third to the ninth irradiations, the sample was irradiated for one second intervals with the beam off for three seconds. This pulse technique was adopted so that sample heating by the electron

beam could be minimized. The pulses were concentrated by the Gralab timer. In the tenth and twelfth irradiations, the sample was irradiated for one second intervals with beam off for four seconds.

## Statement of Errors

Uncertainties may exist in the process of irradiating the sample with the Van de Graaff electrostatic accelerator. The accelerating voltage can be read to about $\pm$ 0.025 MV. Consequently, the electron energy has an uncertainty of $\pm$ 1.4 %. The beam current meter can be read to about 0.1 $\mu$A; however, sometimes the current drifts $\pm$ 0.5 $\mu$A during an irradiation. We estimate the uncertainty in the beam current to be $\pm$ 5 %. The irradiation time has been controlled by a Gralab Model 900 programable timer that is accurate within $\pm$ 0.015 % at one minute. But the rising and falling time of the beam current is considered to be around 10 ms which gives the uncertainty of 1 %. the error due to the adjustment of the accelerator voltage, the beam current, and the irradiation time turns out to be about $\pm$ 7.5 %. Uncertainties may have occured in the placement of the sample in front of the Van de Graaff window. The sample was placed 12.7 cm (5 inches) from the window. We estimate the uncertainty in the position to be $\pm$ 0.5 cm for a 3.9 % error. However, it does not affect the overall error of the radiation dose very much since the irradiation energy is expected to change a little due to the distance of 12.7 cm apart. Thus, the total error in the radiation dose is estimated to be $\pm$ 8 % to $\pm$ 10 %.

The cleaning and mounting techniques were developed to minimize their effect on the acoustic loss. Since we typically achieve acoustic Q's, $> 10^7$, at 5K we are reasonably certain that the holder and cleaning

procedures are not limiting the measurement at higher temperature.

The Lake Shore's Model DRC-80 thermometer and controller displays temperature accurately with $\pm$ 0.5K from 4K to 330K. The temperature was increased in a rate of 0.13K/minute during the measurements, and so the displayed temperature was not exactly same as the sample's temperature.

Finally the error of the acoustic loss measurement can be occurred due to the reading error of the decay time, $T_{\frac{1}{2}}$, and the tuning error of the resonance frequency. The frequency can be adjusted within $\pm$ 5Hz. But this frequency error does not make a big difference in the calculation of the acoustic loss. The decay time was not stable but fluctuated within $\pm$ 0.5 ms at $T_{\frac{1}{2}}$ = 10 ms or $\pm$ 1 ms at $T_{\frac{1}{2}}$ = 20 ms approximately. The uncertainty of the acoustic loss measurement is expected to be $\pm$ 4.8 %.

# CHAPTER III

## RESULTS AND DISCUSSIONS

Figure 8 shows the acoustic loss versus temperature spectra for the
the unswept Toyo Supreme Q resonator blank in the as-received state and
after irradiations of 60 seconds and 330 seconds. Nine other spectra
were measured for irradiations ranging from 2 seconds to 270 seconds.
These curves were omitted for the purpose of clarity. The curve for the
as-received state shows the expected thermal phonon background [2] with
a large 54K Al-Na$^+$ peak superimposed on it. A much smaller Al-Na$^+$
related peak is also present at 135K. Interfering modes were also ob-
served in the region between 100K and 200K. The 54K loss peak has a
height, $\Delta Q_{54}^{-1}$, of 5.63 x 10$^{-5}$. Samples from Toyo bar, SQ-B, contain 10
to 15 ppm aluminum as impurities and a previously measured Na$^+$-swept
SQ-B resonator blank shows the 54K loss peak with $\Delta Q_{54}^{-1} = 2$ x 10$^{-4}$.
The concentration of the Al-Na$^+$ centers for the unswept SQ-B is estimated
to be about 3 ppm from the Equation;

$$C = [ 5 ( \pm 20 \% ) \times 10^4 ] \cdot \Delta Q_{54k}^{-1} \tag{18}$$

where C is in ppm and $\Delta Q_{54k}^{-1}$ is the height of the 54K loss peak [11].
Thus, about 1/5 to 1/3 of the 10 to 15 ppm Al sites are compensated by
the interstitial Na$^+$ ions and the remaining aluminum must be compensated
by interstitial Li$^+$ ions. No Al-OH$^-$ centers are observed unless the
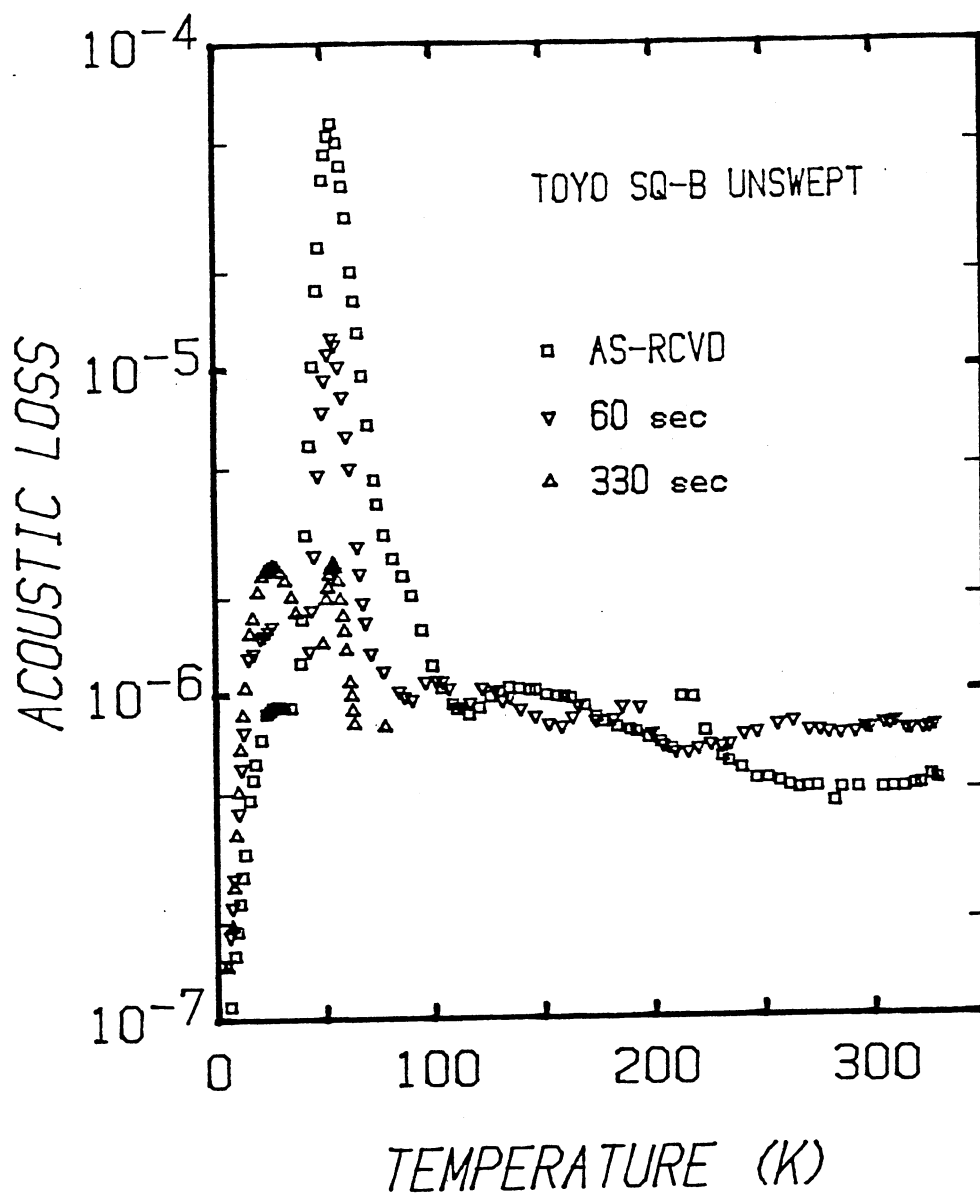sample has been air/hydrogen swept or irradiated.

Figure 8. The Acoustic Loss versus Temperature Spectra for
Unswept Blank, SQ-B, before a Room Temperature
Irradiation and after 60, and 330 Seconds
Irradiations at Room Temperature

The loss spectrum for the partially irradiated sample after the pulsed 60 sec dose shows that the 54K Al-Na$^+$ peak was reduced to about 20 % of its initial value and that loss peaks at 23K and 335K were introduced by the irradiation. The 23K peak [14] is related to the Al-hole center. Interfering modes were still observed. The new 23K and 335K loss peaks indicate that the Al-hole centers and as-yet unknown defect centers has been created respectively by the low-level dose of the room temperature irradiation. The concentration of the Al-Na$^+$ centers were reduced to 0.6 ppm from 3 ppm. The Al-Na$^+$ and Al-Li$^+$ centers were converted into a mixture of Al-hole and Al-OH$^-$ centers by the irradiation [21]. Further pulsed irradiation as shown by the 330 seconds curve reduced the 54K loss peak to about $1.63 \times 10^{-6}$ and increased the 23K loss peak to about $1.58 \times 10^{-6}$. The concentration of the Al-Na$^+$ centers was reduced to about 0.09 ppm due to the destruction of the Al-Na$^+$ centers.

The 100K and 135K Al-hole [12, 13, 14] loss peaks are small and the interfering modes persisted around these temperatures throughout the experiments while the 23K loss peak responds well to the production of the Al-hole defect centers following the low-level dose of irradiation at room temperature. Therefore, the 23K and 54K loss peaks were used to monitor the production of Al-hole centers and the destruction of the Al-Na$^+$ centers respectively as functions of the low-level dose of irradiation at room temperature. Figure 9 shows the 23K peak height, $\Delta Q_{23k}^{-1}$, and 54K peak height, $\Delta Q_{54k}^{-1}$, vs irradiation time curves. 40.4 % of the original 54K loss peak in reference to the 330 seconds irradiation was sharply removed by the 10 seconds irradiation and 81.5 % of the original 54K peak by the 60 seconds irradiation. It smoothly goes down from the
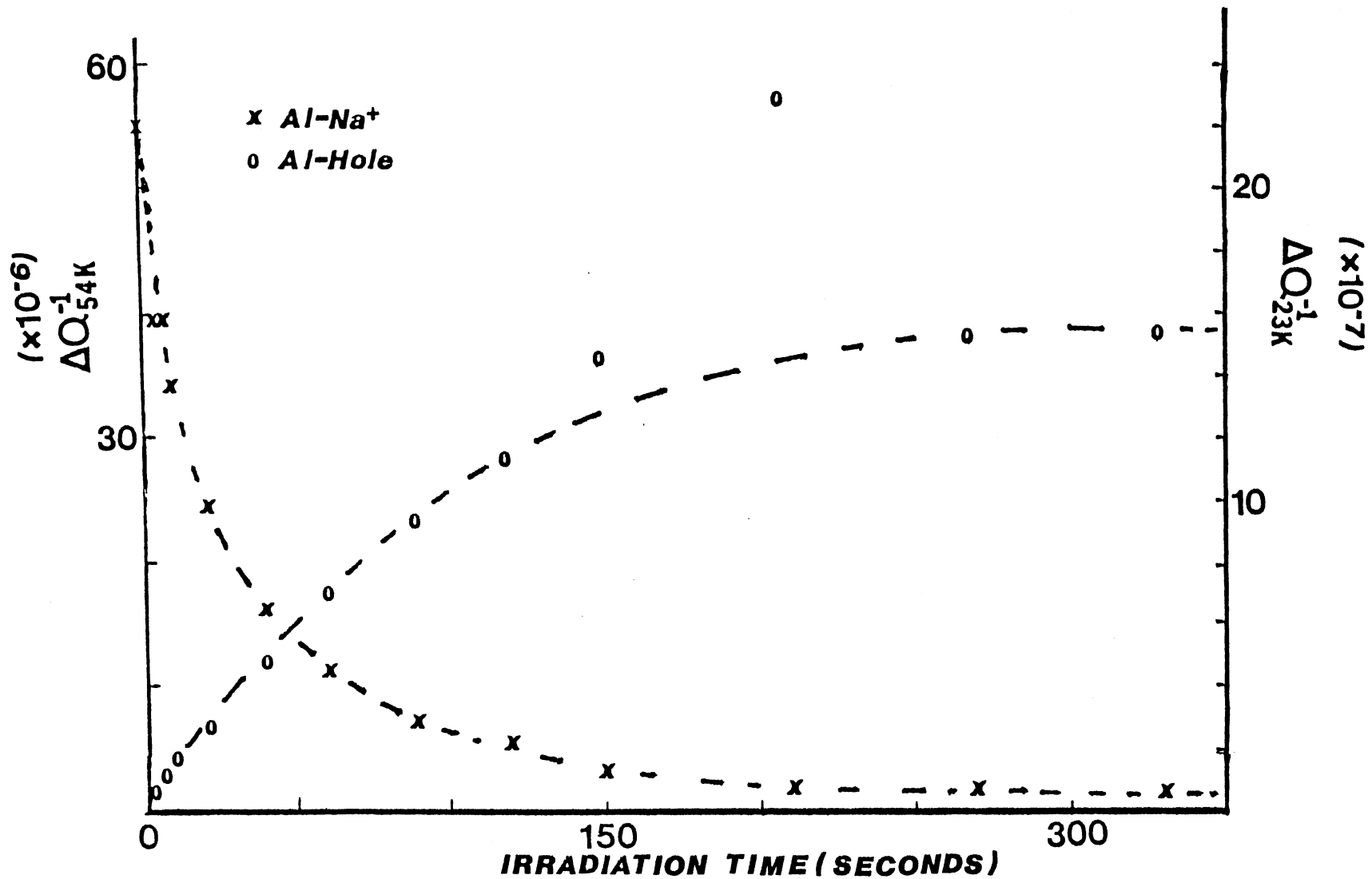
Figure 9. The Height of the 23K and 54K Loss Peaks versus Irradiation Time Curves.
The Al-hole Curve grows in smoothly while the Al-Na$^+$ Curve decreases

60 seconds to 210 seconds irradiation and starts to be saturated at about 210 seconds irradiation. These results suggest that the 81.5 % of the Al-Na$^+$ centers has been destroyed with the low-level dose of the room temperature irradiation for 60 seconds. The 23K Al-hole center loss peak increases rapidly during the initial irradiations and then slows. It saturates near 250 seconds. The 54K Al-Na$^+$ center peak mirrors this process in the sense that it shows an initial rapid de-crease and is nearly completely removed by the time the Al-hole peak reaches saturation. These results suggest that the production of the Al-hole centers is clearly related to the destruction of the Al-Na$^+$ centers. It is now known that the room temperature irradiation to the saturation converts about 25 % of the Al sites into the Al-hole centers and 75 % of the Al sites into the Al-OH$^-$ centers [21]. Therefore, the production pattern of the Al-hole centers follows the destruction pat-tern of the sum of the Al-Li$^+$ and Al-Na$^+$ centers. Since approximately 77 % of the Al sites for the unswept sample, SQ-B, are compensated by the Li$^+$ ions, the destruction pattern of the Al-Li$^+$ centers is also ex-pected to follow closely the production pattern of the Al-hole centers. The results of Hitt and Martin [19] and Martin [20] suggest that both the Al-Na$^+$ and Al-Li$^+$ centers have similar behavior during irradiation at room temperature. Consequently, we assume that the Al-Li$^+$ concen-tration tracks with the Al-Na$^+$ curve as shown in Figure 8. Other works done by J. J. Martin [20] shows that the Al-OH$^-$ centers also start to be produced by the small dose of the room temperature irradiation and grow up smoothly as does the Al-hole 23K peak curve following the irradiation. Both the Al-hole and the Al-OH$^-$ centers start to be produced with the low-level dose of irradiation at room temperature.

The acoustic loss spectra shown in Figure 8 have an interesting irradiation-time dependence. While our measurements only went to 330K, the results strongly suggest the presence of a loss peak near 335K [20]. This peak seems to reach maximum strength at 10 seconds irradiation time and then decreases for the subsequent irradiation. It can be understood as follows. The freed $Na^+$ ions from the $Al-Na^+$ centers are trapped in unknown sites and produce new $X-Na^+$ defect centers, where X represents an unknown site. It does not go up high like the 54K loss peak because the concentration of the X sites is lower than that of the Al sites. It goes down again since the $X-Na^+$ centers are destroyed by the room temperature irradiation.

# CHAPTER IV

## CONCLUSIONS

Approximately 81.5 % of the Al-Na$^+$ centers were destroyed with the 60 seconds irradiation at room temperature. Both the removal of the 54K Al-Na$^+$ loss peak and the production of the 23K Al-hole loss peak start to saturate after about 200 seconds irradiation time. No "steps" were observed in the production curves. Like the Al-OH$^-$ center, the Al-hole center grows in smoothly as the Al-Na$^+$ and, probably, Al-Li$^+$ centers are removed with the room temperature irradiation. The destruction pattern of the Al-Li$^+$ centers is expected to follow closely the production pattern of the Al-hole centers which is similar to the destruction pattern of the Al-Na$^+$ centers. Therefore, the Al-Li$^+$ center tracks with the Al-Na$^+$ curve as shown in Figure 8.

The loss peak near 335K grows and then decays as the radiation dose increases. The 335K loss peak is considered to be caused by an unknown defect center, X-Na$^+$.

REFERENCES

[1] Cady, W. G. <u>Piezoelectricity</u>, Vols. I and II (Dover Publications, New York, 1964).

[2] Fraser, D. B. <u>Physical Acoustics</u>,Vol. 5, W. P. Mason Ed. (Academic Press, New York, 1968), pp. 59.

[3] Nowick, A. S. and Berry, B. S. <u>Anelastic Relaxation in Crystalline solids</u> (Academic Press, New York, 1972).

[4] Kittel, C.; Knight, W. D.; and Ruderman, M. A. <u>Mechanics</u>, (Mcgraw-Hill, 1973)

[5] Bömmel, H. E.; Mason, W. P.; and Warner, A. W. Phys. Rev.,<u>99</u>,1894, (1955).

[6] Bömmel, H. E.; Mason, W. P.; and Warner, A. W. Phys. Rev., <u>102</u>,64, (1956).

[7] King, J. C. Bell System Tech. J., <u>38</u>, 573, (1959).

[8] King, J. C. Final Rept. DA 36-039 SC-64586, Bell Telephone Lab. Inc., (1960).

[9] Jones, C. K. and Brown, C. S. Proc. Phys. Soc. (London), <u>79</u>, 930, (1962).

[10] Fraser, D. B. J. Appl. Phys., <u>35</u>, 2913, (1964).

[11] Martin, J. J. Proc. of 38th Annual Symposium on Frequency Control, 16, (1984).

[12] King, J. C. and Sander, H. H. IEEE Trans. Nucl. Sci., <u>NS</u>-19, 23, (1972).

[13] Martin, J. J.; Halliburton, L. E.; and Bossoli, R. B. Proc. of 35th Annual Symposium on Frequency Control, 317, (1981).

[14] Martin, J. J. and Doherty, S. P. Proc. of 34th Annual Symposium on Frequency Control, 81, (1980).

[15] Sibley, W. A.; Martin, J. J.; Wintersgill, M. C.; and Brown, J. D. J. Appl. Phys. <u>50</u>, 5449, (1979).

[16] Markes, M. E. and Halliburton, L. E. J. Appl. Phys., <u>50</u>, 8172, (1979).

[17] Doherty, S. P.; Martin, J. J.; Armington, A. F.; and Brown, R. N. J. Appl. Phys., $\underline{51}$, 4164, (1980).

[18] Berry, B. S. and Nowick, A. S. <u>Physical Acoustics</u>, Vol. III, Part A, W. P. Mason Ed. (Academic Press, New York, 1966).

[19] Hitt, K. B. and Martin, J. J. J. Appl. Phys., $\underline{54}$, 5030, (1983).

[20] Martin, J. J. (Private Communication), Mar. 1985, Oklahoma State University, Professor.

[21] Halliburton, L. E.; Koumvakalis, N.; Markes, M. E.; and Martin, J.J. J. Appl. Phys., $\underline{52}$, 3565, (1981).

VITA 2

Ho Byong Hwang

Candidate for the Degree of

Master of Science

Thesis:  RADIATION EFFECTS IN THE ACOUSTIC LOSS SPECTRA OF AT-CUT
TOYO QUARTZ CRYSTAL

Major Field:  Physics

Biographical:

Personal Date:  Born in Kimjae, Jeonbug, Korea, September 6, 1951,
The son of Jongkyu and Jeongae Hwang.  Married to Meeyoung
Lee on June 8, 1980.

Education:  Graduated from Jeonju Haesung High School, Jeonju,
Jeonbug, Korea in February, 1969; received Bachelor of Science
degree in Physics from Jeonbug National University in February,
1974; attended Graduate School of Jeonbug National University
from March, 1974 to July,1974 and from September,1975 to Feb-
ruary, 1977; attended the University of Kansas from August,
1979 to May, 1981; Completed requirements for degree of Master
of Science at Oklahoma State University in May, 1985.

Professional Experience: Teaching Assistant, Department of Physics,
The University of Kansas, August, 1980 to May, 1981; Teaching
Assistant, Department of Physics, Oklahoma State University,
August, 1981 to December, 1983; Research Assistant, Department
of Physics, Oklahoma State University, January, 1984 to present.